IASS 2023
July 10–14 Melbourne
Integration of Design and Fabrication

Proceedings of the IASS Annual Symposium 2023
Integration of Design and Fabrication
10 – 14 July 2023, Melbourne, Australia
Y.M. Xie, J. Burry, T.U. Lee and J. Ma (eds.)

Local optimization of self-supporting shell structures in 3D printing: a skeleton method

Yefan ZHI[*,a], Hua CHAI[a], Teng TENG[a], Masoud AKBARZADEH[a,b]

[a] Polyhedral Structures Laboratory, Weitzman School of Design, University of Pennsylvania, Philadelphia, USA
Pennovation Center, 3401 Grays Ferry Ave. Philadelphia, PA, 19146
[*] yefanzhi@upenn.edu

[b] General Robotic, Automation, Sensing and Perception (GRASP) Lab, School of Engineering and Applied Science, University of Pennsylvania, Philadelphia, USA

Abstract:

This paper presents an optimization method to create self-supporting shell structures for 3D printing (3DP) purposes. Compared to other methods of construction, 3DP can facilitate the fabrication of freeform, complex shell structures. However, for objects printed at the architectural construction scale, the 3DP supports are typically hard to remove, causing considerable material and energy waste and requiring additional postprocessing work. Making the geometry self-supporting is a challenging alternative to neutralize these downsides of 3DP.

We propose a post-slicing optimization method to make porous shell structures self-supporting for 3DP by reducing the overhang when necessary. The method is applicable to shell structures that, when printed, only consist of walls without infills or caps. After slicing, we represent the planar wall toolpaths using medial axes and maximal disks. The method then examines the proximity between the medial axes of adjacent layers to build a skeleton model and makes adjustments when the overhang exceeds a limit. Finally, the planar toolpaths are updated through linkage to the medial axes. An example of a Triply Periodic Minimal Surface (TPMS) geometry is illustrated.

In this paper, we offer a computational framework for the local optimization process. Instead of imposing limitations at the beginning of the design process, it adjusts a finished design to form self-supporting geometry. It investigates the geometry through an organized series of toolpaths and preserves the shell structure's local thickness and curvature continuity. While recent self-supporting optimization research mainly inspects geometries of fixed vertical sections, our method fully develops 3DP's potential in manufacturing free-form shell structures and can be of vast application on various scales.

Keywords: 3D printing, shell structure, structural optimization, Hangai Prize applicant.

1. Introduction

1.1. Self-supporting structures for architectural additive manufacturing

Additive manufacturing, primarily 3D Printing (3DP), has revolutionized the way objects of different scales are designed and manufactured. It gives architects the ability to flexibly create complex functional and exotic geometries that are difficult to achieve with traditional manufacturing methods [1]. However, architectural additive manufacturing, with concrete 3DP as a most prevalent practice, also faces

Copyright © 2023 by Yefan ZHI et al. Published in the Proceedings of the IASS Annual Symposium 2023 with permission.

limitations in mass production. While conventional layer-based 3DP utilizes support structures that are printed together with the geometry and removed afterward, at the architectural construction scale they are typically hard to remove and create considerable material and energy waste and require additional post-processing work [2].

Overhanging, hole, and edge features in the print geometry usually require support structures [3]. This paper is situated in the trend of designing self-supported structures and neutralizing the downsides of support structures. Making the geometry self-supporting is a challenging task. Extensive research has been conducted to globally optimize the topology using methods involving moving morphable components [2, 4, 5]. However, instead of being the *post-processing* to a pre-designed geometry, the *global* topology optimization process incorporating self-supporting constraints is more like the *design process* itself. The principles of topology optimization restrict the freedom of architects in experimenting with novel structural prototypes. Their outcomes are usually limited to multifurcating structures with fixed sections such as the Messerschmitt–Bölkow–Blohm (MBB) beam.

In this paper, we propose an alternative to creating a self-supporting structure by locally optimizing a present geometry that is in general printable but can be vulnerable at certain locations. The main characteristics of a vulnerable region in the print are identified as bridges, overhangs, and angles [6] when the geometry is viewed *as geometry*, or in other words, the mesh or boundary representation as the slicing input. Our method will scrutinize the geometry *as toolpaths* after the conventional slicing is finished. The unprintable characteristics, all referred to as *overhangs* in this paper, will then be manifested as the planar offset between layers of toolpaths. Utilizing a post-slicing skeleton model we will be able to calculate and reduce the overhangs when necessary and thus make the geometry self-supporting.

1.2. 3D printed shell structures

The process of 3DP is essentially linear extrusions. Compared to the traditional casting method, it is advantageous in creating shell structures with holes and multifurcations which then become innovative architectural components such as the wall, column, beam, and dome elements with tailored functions [7–11]. This sustainable approach with minimized material usage to design and fabricate lightweight structures with high structural performance has thus gained more attention.

This paper will look at lightweight porous shell structure components that, when printed in concrete, only consist of walls without infills or caps. Typically they are prefabricated in the factory and then transported to the site for assembly, as opposed to the other two fashions of 3D printing formworks or an entire building [12]. When combined with structural form-finding, they make efficient discrete systems [13]. Triply Periodic Minimal Surface (TPMS), as one of the lightweight structural prototypes, has been extensively tested and researched. Due to their minimal surface area, TPMS structures possess a high surface area-to-volume ratio. The periodic and continuous nature of TPMS structures also allows the efficient distribution of external loads throughout the material. When a force is applied to one point on the structure, the load is distributed across multiple points, reducing the overall stress experienced by any single point. This distribution results in better overall mechanical stability and resistance to deformation [14]. This paper uses Diamond TPMS as a case study and demonstrates the respective potential of our optimization proposal.

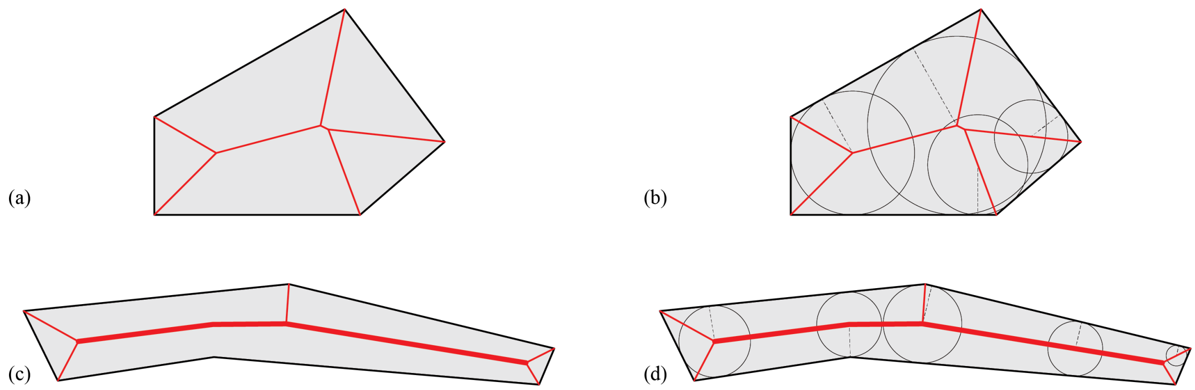

Figure 1: Medial axis (red) and some maximal disks of (a) (b) a regular polygon; and (c) (d) a slender polygon.

1.3. Medial axis and skeleton model

Introduced by Blum [15] in 1967, the *medial axis* is an efficient way to describe a 2D shape. It is essentially the set of points in a shape that have at least two closest points on the shape's boundary (Figure 1a, c). For each point on the medial axis, a unique *maximal disk* can be drawn if we use the distance between that point and the closest points on the boundary as its radius (Figure 1b, d). The points in all the maximal disks are within the original shape and all the points in the original shape are covered by some maximal disks. We call the combination of the medial axis and each point's local radius (of its maximal disk) a *disk representation* of the shape. We can mutually transform between the boundary representation and the disk representation of the original shape. This method is also applicable to planar domains with holes [16] where instead of being a *tree*, the medial axis will incorporate *cycles*.

This paper proposes printing the two sides of shell structures in two parallel curves so that the toolpaths a) are closed contours with seams for better finishing quality and b) can be continuous while accommodating multifurcations in the plane. To do so, the input geometry is a shell with thickness and volume. Given a printing direction (z-axis of the printer), it is sliced into one or multiple closed contours in each plane. If the structure is in general printable, the contours enclose slender domains representing the solid part of the shell (gray parts in 4). Figure 1c, d show that for a slender domain, a main axis (thickened) representing the direction and position of the geometry is observed. It offers an efficient representation where the radii of most maximal disks are similar. Thus we transfer the slender domains created into medial axes for optimization. And the disk radii are recorded as vectors to preserve the shell structure's local thickness and curvature continuity in our method.

The precise calculation of medial axes in polygonal or curved shapes is a complex and slow task [17]. We use an approximate method to compute medial axes and then examine the proximity between the medial axes of adjacent layers. Adjustments are made when the overhang exceeds a limit. Finally, the planar toolpaths are updated through vector linkages to the medial axes. This *skeleton* method will be explained in detail in the Methodology section. Note that while the concept skeleton is used by computer scientists as an extension of the medial axis of a 2D geometry, this paper uses it to refer to an entire 3D print geometry organized in a hierarchical data structure.

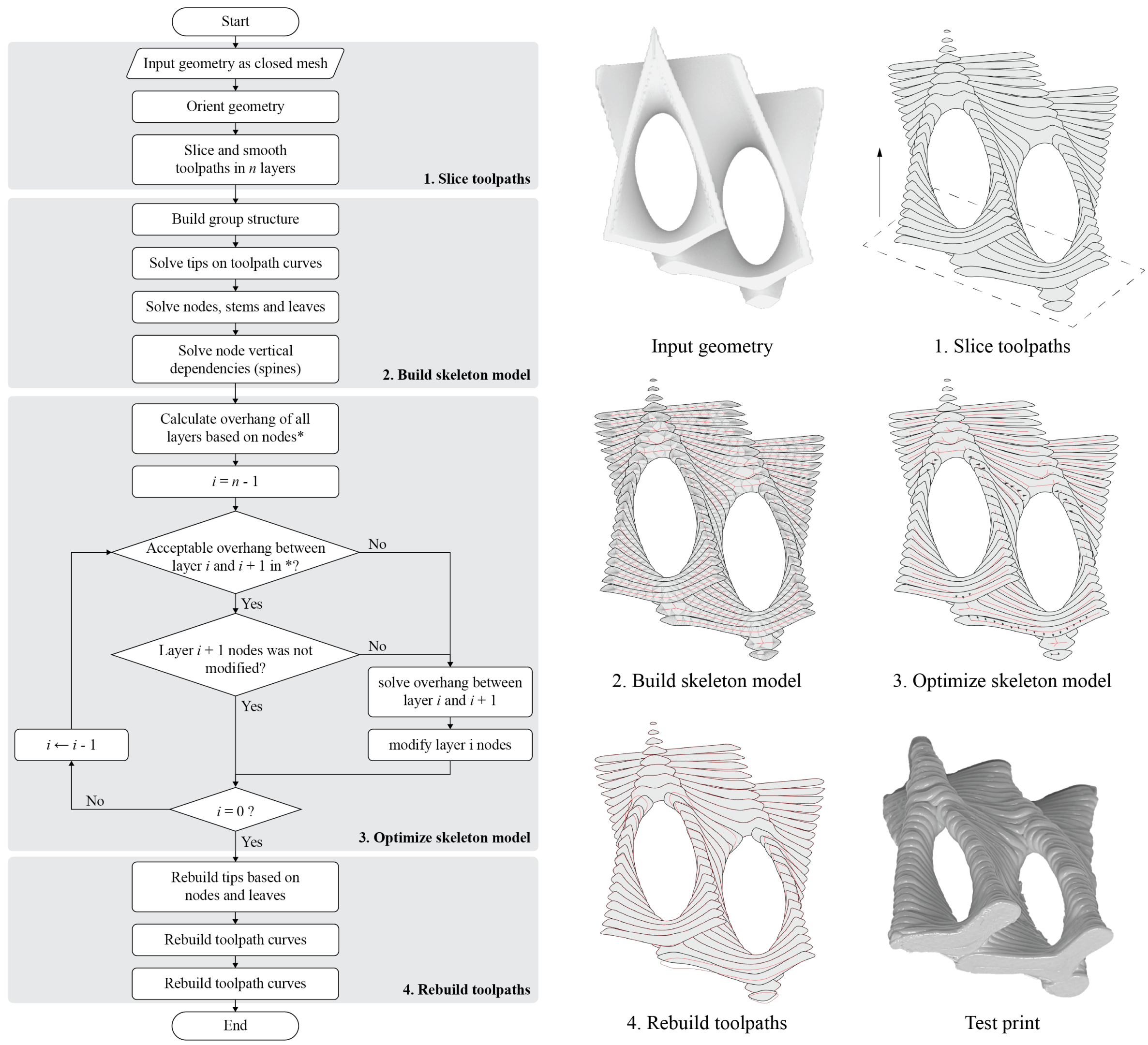

Figure 2: The computational flowchart for reducing the print overhang utilizing the skeleton model method, showing the geometry at different stages.

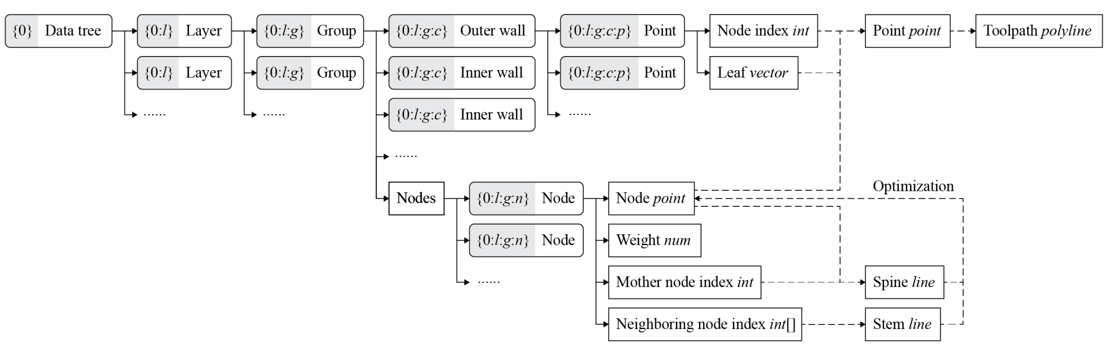

Figure 3: Main data structure of the geometry optimization.

2. Methodology

Figure 2 offers an overview of the optimization framework. It comprises four major steps: slice toolpaths; build the skeleton model; optimize the skeleton model; and finally, rebuild the toolpaths. Figure 3 illustrates the computational data structure where points are stored in relative positions to nodes of the medial axes. A case study of a Triply Periodic Minimal Surface (TPMS) geometry (Figure 2b) generated using the volumetric modeling plugin *Axolotl* [18] for *Grasshopper* is illustrated.

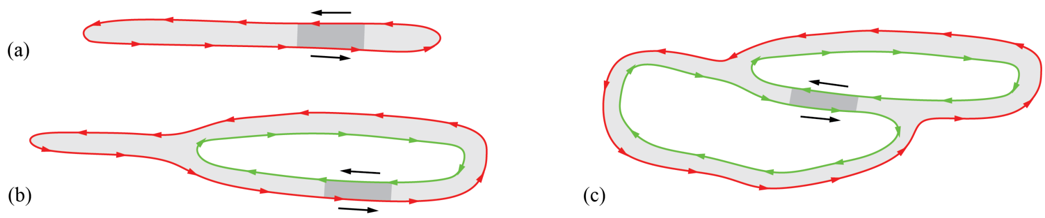

Figure 4: Outer walls (red, counterclockwise) and inner walls (green, clockwise) of groups with (a) no holes; (b) one hole; and (c) multiple holes.

2.1. Slice toolpaths

Our method applies to both parallel and non-parallel slicing of solid geometries. A concrete 3DP geometry as a structural component usually uses its flat top and bottom faces as contact surfaces for assemblage. The two faces are part of the input of the slicing or can be found using a convex hull analysis. They determine the slicing planes in between that intersect the geometry to create closed contour curves.

2.2. Build skeleton model

In each plane or *layer*, the contours are then sorted based on their cross-inclusion relations to form several *groups*. As illustrated by Figure 4, each group indicates a solid domain (shown as gray). A group is formed by one *outer wall* and can have several *inner walls* each indicating a hole. In the data tree, they form a list of curves where the outer wall is the first curve (Figure 3). The printing directions of the walls are also unified to have the parallel layers printed in reversed directions and thus have increased bounding.

Our approach to calculating the medial axis is developed based on the Voronoi diagram approximation method by Brandt and Algazi [19]. (Another application of the method in 3DP is the extrusion rate control to create variable print width [20].) We start by refitting the *toolpath curve* using a compact polyline whose adjacent vertices have a prescribed maximal distance. The vertices are then extracted as a list of *points* (Figure 5a). Based on the discrete points a Voronoi diagram can be solved and purged to show the inner structure of the domain (Figure 5b). The half cells form a redundant, approximate planar skeleton structure. We then merge the adjacent vertices of the Voronoi diagram within a tolerance into *nodes* to make the representation more efficient (Figure 5c). The end nodes (having only one neighbor) too close to the boundary are also purged recursively to extract only the “bones” of the slender geometry. Referring to the original Voronoi diagram, the linkages between nodes are calculated as *stems*. With the node-stem structure formed, each toolpath point is projected to the closest node and regarded as offsetted from it by a *leaf* vector (Figure 5d). Note that here we use nouns describing plants because our geometric structure is similar to plants such as shameplants and ferns in plane.

To examine the overhang between layers, we solve the vertical dependencies between nodes of adjacent layers. When the supporting condition of a node is examined, the node is referred to as the *daughter node*. For each daughter node, the closest node in the previous layer is found as its *mother node*. The last component of the skeleton mode, the *spines* are then created by connecting the daughter nodes and their mother nodes (Figure 5e).

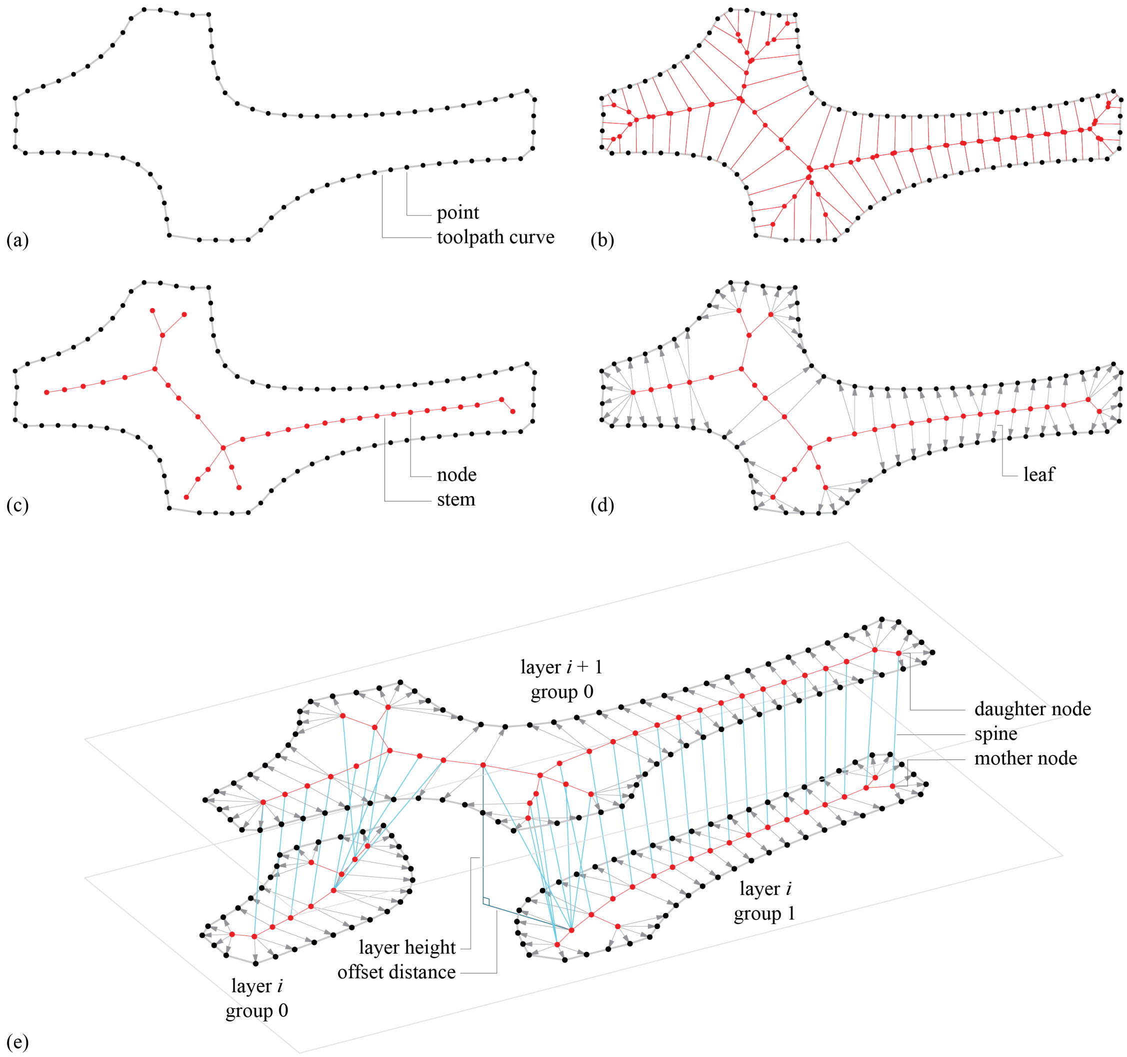

Figure 5: Skeleton model building process: (a) convert the input *toolpath curve* into a compact polyline and extract *points*; (b) solve the Voronoi diagram and the vertices inside the domain; (c) merge the vertices to create *nodes*, purge those too close to the boundary, and create *stem* connections between nodes; (d) find the closest node to each point to create *leaf* vectors; and (e) find each *daughter node* in layer $i+1$ the closest *mother node* in layer i and connect them to form *spines*.

2.3. Optimize skeleton model

The goal of our local optimization method is to reduce overhang between layers. Ideally, the local overhang distance is defined as the offset distance between the new toolpath and the previous one that supports it (Figure 6). It can be calculated by projecting a point on the new toolpath to the previous slicing plane and finding its distance to the closest toolpath curve. We use pairs of mother and daughter

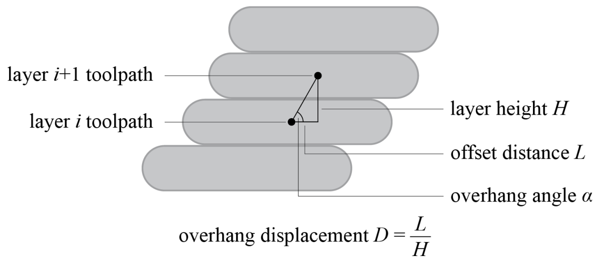

Figure 6: Ideal definition of overhang displacement.

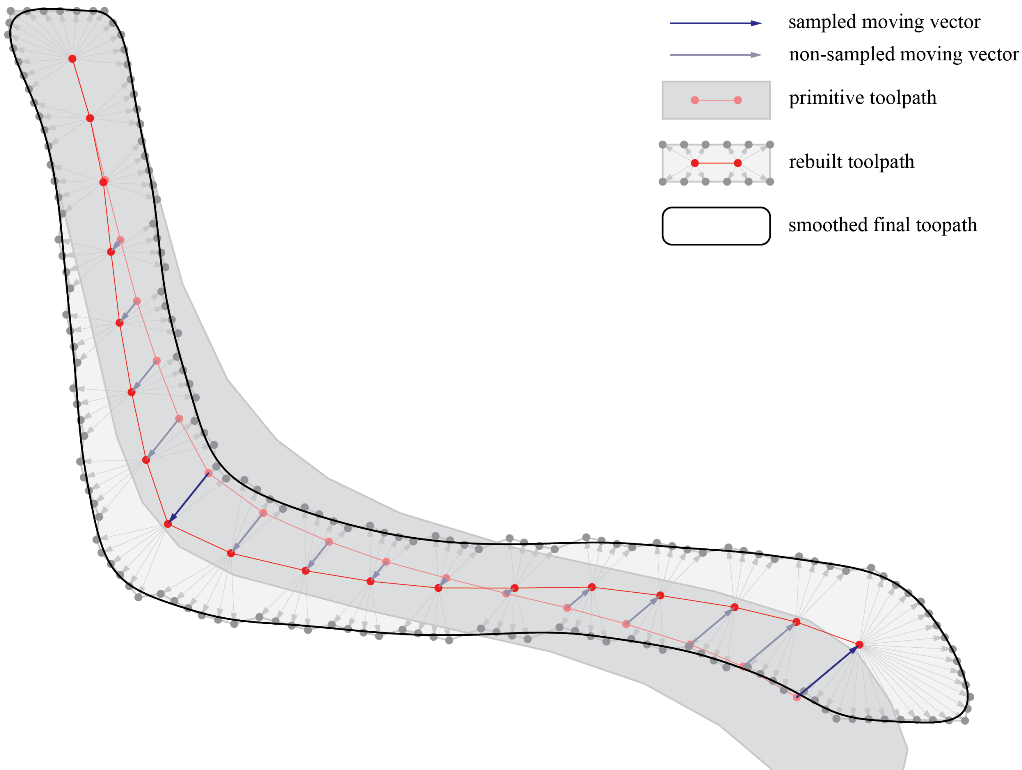

Figure 7: Example of optimizing a group where two nodes are sampled.

nodes, instead of the points to calculate the offset distance and the overhang displacement. The offset distance of all the points that rely on the same daughter node is thus treated as the projected length of the node's spine in the mother layer plane (Figure 5e). Note that the radii of the two nodes also affect the actual offset distance. However when the radius is significantly larger than half of the shell thickness, it means the surface orientation is largely tilted, and in this extreme case allowing more tolerance in offset by neglecting the change in radii can help maintain the overall shape of the geometry.

Our method requires a predetermined overhang displacement optimization goal (0.9 in the case study). As shown by Figure 2a, after a round of pre-check, the local optimization process examines each layer in a certain order. Usually, the contact surface of the top and bottom faces should be preserved in their original shapes and the merging regions close to the top are more dangerous than the diverging regions close to the bottom. Therefore, our method follows a top-down order in inspecting layers.

Examining each pair of adjacent payers, we adjust the mother layer (layer i) to better support the daughter layer (layer $i+1$). Each mother node receives *moving vectors* required by the daughter nodes to reduce their overhang displacement when necessary. One mother node can have multiple daughter nodes. The vector with the largest magnitude is used to move the mother node, which means that at times our method cannot eliminate all excessive overhangs.

A node is *sampled* if it received a moving vector as the mother node. However, its neighbors should also be adjusted to preserve curvature continuity. The moving vectors of the *non-sampled* nodes are calculated based on their distance to the sampled nodes. The distance is the length of the path between the two nodes on the graph formed by nodes and stems. It acts as a variable to linearly reduce the sampled moving vector in solving non-sampled moving vectors. In the example of Figure 7, only two mother nodes are sampled, meaning their overhangs exceed the prescribed limit. When we tune the nodes in a continuous way using both sampled and non-sampled moving vectors, the curvature continuity of the node-stem graph is preserved as in the original geometry.

2.4. Rebuild toolpaths

The rebuilding of toolpaths is straightforward. By adding back the leaf vectors to the new nodes, the points of the new curves are recomputed as shown in Figure 7. The rebuilt toolpath is then smoothed recursively to form the final toolpath. The entire optimization process thus mimics the kinematics of a snake skeleton and the thickness and curvature continuity is preserved in the new shell walls.

3. Results

Our case study features a $35 \times 70 \times 70$mm Diamond TPMS with a 2mm thickness as the input geometry. We use an in-house developed PET-G printer with a 1.65mm diameter nozzle to simulate the concrete 3DP in a $1/10$ scale. The print width is 2mm and the layer height is 1mm. 0.9 is set as the optimization threshold. The computation process of slicing and optimizing takes around 60 seconds.

The primitive and optimized toolpaths differ mainly in merging regions (Figure 8a). The branches holding the bridge are dragged towards each other to reduce the overhang (Figure 8b, d). Figure 8c shows the cumulative distribution of the overhang. The overhang at each node is weighted by the length of the toolpath projected to it. As a result, the percentage of toolpaths sufficing the requirement of 0.9 raised from 91% to 99%.

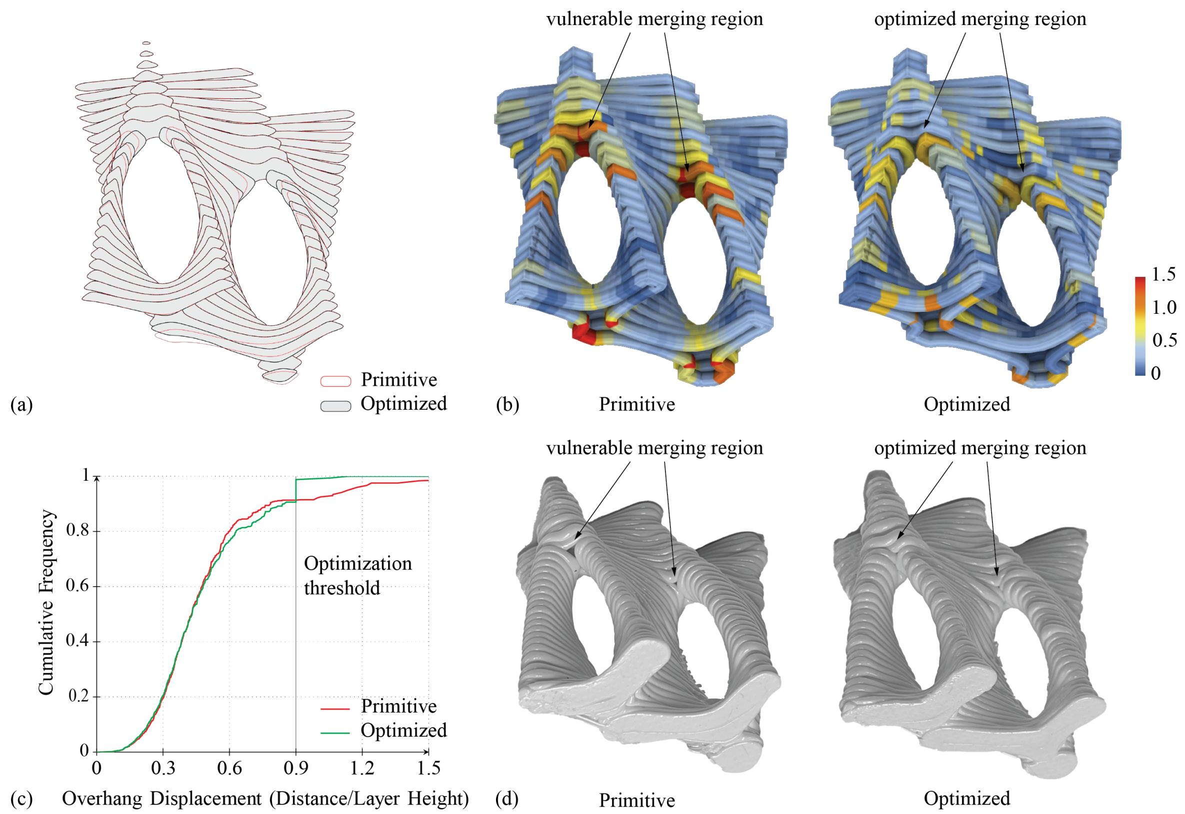

Figure 8: Optimization results of a Diamond TPMS geometry, 0.9 is set as the maximal overhang displacement: (a) toolpaths; (b) volumetric visualization showing overhang displacement; (c) cumulative distribution of printing overhang displacement; and (d) test prints.

4. Conclusion

In this paper, we offer a computational framework for the local optimization process. Instead of imposing limitations at the beginning of the design process, it adjusts a finished design to form self-supporting geometry. It investigates geometry through an organized series of toolpaths. It is a pivot exploration to assist in manufacturing free-form shell structures and can be of vast application on various scales. Meanwhile, it has the following limitations that require future work:

The method is highly resolution-dependent. The resolution and tolerance parameters, especially the overhang threshold, determine the quality of the optimized print. When the method is applied to different scales and diverse geometries, a systematic study of those parameters is required.

While our method features a top-down sequence, the order in which the layers should be organized and optimized is still open to discussion. One possible solution is to relate the overhang message with the Reeb graph structure of the geometry and decide on an optimization sequence accordingly. (An application of the Reeb graph in 3DP is provided by [21].) In addition, a constraint over the geometry's boundary parts is also a feature required by using such prints as structural components.

Finally, our local optimization can change the force flow and thus the structural performance of prints. A comprehensive, comparative study is required to investigate its limits and downsides. Cracking and vibration in the printing process of branching shell structures, discussed by [22], is also another factor affecting the printability and final quality that need to be evaluated in addition to being self-supported.

Acknowledgements

The authors gratefully acknowledge the support provided by the Advanced Research Projects Agency – Energy (ARPA-E) Grant of U.S. Department of Energy (DE-AR0001631), the National Science Foundation CAREER Award (NSF CAREER-1944691 CMMI), and the National Science Foundation Future Eco Manufacturing Research Grant (NSF, FMRG-CMMI 2037097) awarded to Dr. Masoud Akbarzadeh.

References

[1] B. Khoshnevis, "Automated construction by contour crafting—related robotics and information technologies," *Automation in Construction*, 2004.

[2] K. V. Bhat, G. Capasso, S. Coniglio, J. Morlier, and C. Gogu, "On some applications of generalized geometric projection to optimal 3d printing," *Computers & Graphics*, vol. 102, pp. 199–212, 2022.

[3] J. Jiang, X. Xu, and J. Stringer, "Support structures for additive manufacturing: A review," *Journal of Manufacturing and Materials Processing*, vol. 2, no. 4, 2018.

[4] A. T. Gaynor and J. K. Guest, "Topology optimization considering overhang constraints: Eliminating sacrificial support material in additive manufacturing through design," *Structural and Multidisciplinary Optimization*, vol. 54, pp. 1157–1172, Nov. 2016.

[5] X. Guo, J. Zhou, W. Zhang, Z. Du, C. Liu, and Y. Liu, "Self-supporting structure design in additive manufacturing through explicit topology optimization," *Computer Methods in Applied Mechanics and Engineering*, vol. 323, pp. 27–63, 2017.

[6] M. Fernandez-vicente, M. Canyada, and A. Conejero, "Identifying limitations for design for manufacturing with desktop fff 3d printers," *International Journal of Rapid Manufacturing*, vol. 5, 12 2015.

[7] R. van Woensel, T. van Oirschot, M. Burgmans, M. Mohammadi, and K. Hermans, "Printing architecture: An overview of existing and promising additive manufacturing methods and their application in the building industry," *The International Journal of the Constructed Environment*, vol. 9, pp. 57–81, 06 2018.

[8] C. Gosselin, R. Duballet, P. Roux, N. Gaudillière-Jami, J. Dirrenberger, and P. Morel, "Large-scale 3d printing of ultra-high performance concrete – a new processing route for architects and builders," *Materials & Design*, vol. 100, 03 2016.

[9] A. Anton, E. Skevaki, P. Bischof, L. Reiter, and B. Dillenburger, "Column-Slab Interfaces for 3D Concrete Printing," in *Proceedings of the 42nd Annual Conference of the Association for Computer Aided Design in Architecture (ACADIA)*, 2022.

[10] G. Vantyghem, W. De Corte, E. Shakour, and O. Amir, "3d printing of a post-tensioned concrete girder designed by topology optimization," *Automation in Construction*, vol. 112, p. 103084, 2020.

[11] L. Prasittisopin, T. Sakdanaraseth, and V. Horayangkura, "Design and construction method of a 3d concrete printing self-supporting curvilinear pavilion," *Journal of Architectural Engineering*, vol. 27, no. 3, p. 05021006, 2021.

[12] J. Xiao, G. Ji, Y. Zhang, G. Ma, V. Mechtcherine, J. Pan, L. Wang, T. Ding, Z. Duan, and S. Du, "Large-scale 3d printing concrete technology: Current status and future opportunities," *Cement and Concrete Composites*, vol. 122, p. 104115, 2021.

[13] H. Chai, M. Bolhassani, and M. Akbarzadeh, "Structural form-finding of multi-span undulating funicular beam structure," in *Proceedings of IASS 2022 symposium affiliated with APCS 2022 conference*, (Beijing, China), September 19-22 2022.

[14] Y. Wu, J. Fang, C. Wu, C. Li, G. Sun, and Q. Li, "Additively manufactured materials and structures: A state-of-the-art review on their mechanical characteristics and energy absorption," *International Journal of Mechanical Sciences*, 2023.

[15] H. Blum, "A Transformation for Extracting New Descriptors of Shape," in *Models for the Perception of Speech and Visual Form* (W. Wathen-Dunn, ed.), pp. 362–380, Cambridge: MIT Press, 1967.

[16] H. I. Choi, S. W. Choi, H. P. Moon, and N.-S. Wee, "New algorithm for medial axis transform of plane domain," *CVGIP Graph. Model. Image Process.*, vol. 59, pp. 463–483, 1997.

[17] O. Aichholzer, W. Aigner, F. Aurenhammer, T. Hackl, B. Jüttler, and M. Rabl, "Medial axis computation for planar free–form shapes," *Computer-Aided Design*, vol. 41, no. 5, pp. 339–349, 2009. Voronoi Diagrams and their Applications.

[18] M. Bernhard, M. Hansmeyer, and B. Dillenburger, "Volumetric modelling for 3d printed architecture," in *Advances in Architectural Geometry 2018*, (Göteborg, Sweden), pp. 392–415, 09 2018.

[19] J. W. Brandt and V. Algazi, "Continuous skeleton computation by voronoi diagram," *CVGIP: Image Understanding*, vol. 55, no. 3, pp. 329–338, 1992.

[20] P. F. Yuan, Q. Zhan, H. Wu, H. S. Beh, and L. Zhang, "Real-time toolpath planning and extrusion control (rtpec) method for variable-width 3d concrete printing," *Journal of Building Engineering*, vol. 46, p. 103716, 2022.

[21] I. Mitropoulou, M. Bernhard, and B. Dillenburger, "Nonplanar 3d printing of bifurcating forms," *3D Printing and Additive Manufacturing*, 10 2021.

[22] H. ming Zhao, Y. He, J. zhong Fu, and J. jiang Qiu, "Inclined layer printing for fused deposition modeling without assisted supporting structure," *Robotics and Computer-Integrated Manufacturing*, vol. 51, pp. 1–13, 2018.